QUANTITATIVE 3D INTEGRATION OF ELECTROMAGNETIC AND SEISMIC DATA TO OPTIMIZE STRUCTURAL SIMILARITY INVERSION RESULTS IN OFFSHORE NORTHWEST BORNEO, MALAYSIA

AHMAD SHAHIR BIN SALEH

UNIVERSITI SAINS MALAYSIA

2023

QUANTITATIVE 3D INTEGRATION OF ELECTROMAGNETIC AND SEISMIC DATA TO OPTIMIZE STRUCTURAL SIMILARITY INVERSION RESULTS IN OFFSHORE NORTHWEST BORNEO, MALAYSIA

by

AHMAD SHAHIR BIN SALEH

Thesis submitted in fulfilment of the requirements
for the degree of
Doctor of Philosophy

July 2023

ACKNOWLEDGEMENT

I would like to express my gratitude to the Almighty Allah, for giving me the opportunity to learn useful knowledge. I also thank my supervisors, Dr Nur Azwin Ismail, Dr. Maxwell Azuka Meju and Prof Mohd Nawawi Mohd Nordin for their unrelentless support and guidance towards completion of this study. I also would like to thank my family, especially my wife Pn. Norsilawati binti Ramli and my mother, Pn. Sharifah binti Hamdan for their help in various ways throughout this difficult journey. I thank PETRONAS for providing the geoscience data and providing access to the software and hardware used in this study. Finally, I would like to specially dedicate this thesis to my late son, Ahmad Darwish Haikal bin Ahmad Shahir. My thoughts are always with him. May his soul rests in peace.

TABLE OF CONTENTS

LIST OF TABLES

Page

LIST OF FIGURES

Page

LIST OF SYMBOLS

A	Jacobian, or sensitivity matrix
$\alpha_{h,\,v}$	Regularization weight in horizontal (h) or vertical (v) direction
α_s	Shear impedance – acoustic impedance projection
B	Magnetic flux density (Wb/m^2), or Partial derivatives matrix of cross gradient function
β	Log_{10}(resistivity), or cross-gradient weight
C	Discrete divergence operator defined on primary grid, or Preconditioner matrix
$\tilde{\mathbf{C}}$	Discrete divergence operator defined on dual grid
$\mathbf{C}_d$	Data covariance matrix
$\mathbf{C}_m$	Model covariance matrix
D	Electric displacement (A/m^2), or Diagonal matrix
d	Data vector (linear inversion)
E	Electric field (V/m), or Eigenvalue matrix
e	Error vector
f	Frequency (Hz)
F	Forward modelling operator (nonlinear inversion)
G	Forward modelling operator (linear inversion)
g	Gradient vector
γ	Data weight (in joint inversion)
H	Magnetic field (A/m)
I	Image gradients
J	Electric current density (A/m^2)
K	Regularization operator

M	Model parameter vector (linear inversion)
p	Search direction vector
Q	Eigenvector matrix
R	Rotation matrix operator or first order difference matrix
r	Reflectivity
R_w	Resistivity of formation water (Ohm.m)
S	Discrete curl operator defined on primary grid, or Structure tensor
$\tilde{\mathbf{S}}$	Discrete curl operator defined on dual grid
S	Slowness (s/m) or Seismic trace
t	Time (seconds)
T	Period (seconds), or Tipper (magnetic fields ratio)
v	Magnetic reluctivity (m/H), or Velocity (m/s)
V_p	Compressional (P) velocity (m/s)
V_s	Compressional (S) velocity (m/s)
V_{p0}	Vertical P-wave velocity (m/s)
V_{nmo}	Normal moveout velocity(m/s)
w	Wavelet
W	Inverse data covariance matrix
X	MT signal
$\tilde{\mathbf{X}}$	Despiked MT signal
m	Model parameter vector (nonlinear inversion)
y	Data vector (nonlinear inversion)
Z	Magnetotelluric impedance tensor
β	Conjugate gradient parameter
ε	dielectric permittivity (F/m), or epsilon (seismic anisotropy parameter)

μ	magnetic permeability (H/m)
ρ	Density (g/cc)
ρ_e	Electric charge density (C/m^3)
$m_{h,\,v}$	Horizontal (h) or vertical (v) resistivity (Ohm.m)
α_s	Shear impedance – acoustic impedance projection
$\sigma_{h,\,v}$	Horizontal (h) or vertical (v) conductivity (S/m)
τ	Cross gradient function
ω	Angular frequency (radians per second.)
δ	Skin depth (m), or delta (seismic anisotropy parameter)
γ	Wavenumber (1/m), coherence attribute, or data weight
∇m_{seis}	Gradients from seismic structure tensor analysis

LIST OF ABBREVIATIONS

1D	One dimension
2D	Two Dimensions
3D	Three Dimensions
AFMAG	Audio-frequency Magnetic
AI	Acoustic Impedance
AMT	Audio Magnetotellurics
ATR	Anomalous Transverse Resistance
AVO	Amplitude versus Offset
CDP	Common Depth Point
CMP	Common Mid-Point
CPU	Central Processing Unit
CSAMT	Controlled Source Audio Magnetotellurics
CSEM	Controlled Source Electromagnetic
DRI	Direct Resistivity Indicator
EEI	Extended Elastic Impedance
EI	Elastic Impedance
EM	Electromagnetic
EMGS	Electromagnetic Geoservices ASA
FIT	Finite Integration Technique
FWI	Full Waveform Inversion
GEBCO	General Bathymetric Chart of the Oceans
GI	Gradient Impedance
GPR	Ground Penetrating radar
GPU	Graphics Processing Unit
GUI	Graphical User Interface
HED	Horizontal Electric Dipole
HPC	High-Performance Computer
HS	Hashin-Shtrikman
HTEM	Helicopter Time Domain Electromagnetic
HTI	Horizontal Transverse Isotropy
LFM	Low Frequency Model

LRLC	Low Resistivity Low Contrast
MT	Magnetotellurics
MVO	Magnitude versus Offset
NLCG	Nonlinear Conjugate Gradient
NMO	Normal Moveout
nRMS	Normalized Root Mean Square
OBC	Ocean Bottom Cable
OBN	Ocean Bottom Node
PGS	Petroleum Geo-Services ASA
PSDM	Prestack Depth Migration
PVO	Phase versus Offset
QC	Quality Control
RAM	Random Access Memory
RMEV	Robust Multivariate Error-in-Variables
RMO	Residual Moveout
SI	Shear Impedance
SRME	Surface Related Multiple Elimination
TEM	Time Domain Electromagnetic
TTI	Tilted Transverse Isotropy
VED	Vertical Electric Dipole
VTI	Vertical Transverse Isotropy

LIST OF APPENDICES

INTEGRASI KUANTITATIF 3D BAGI DATA ELEKTROMAGNETIK DAN SEISMIK UNTUK MENGOPTIMUMKAN HASIL PENYONGSANGAN KESAMAAN STRUKTUR DI PESISIR BARAT LAUT BORNEO, MALAYSIA

ABSTRAK

Songsangan 3D data seismik dan elektromagnetik (EM) yang digandingkan dengan kriteria kecerunan silang adalah dikenali dapat memaksimakan ketepatan dan mengurangkan ketidakpastian dalam eksplorasi subpermukaan. Tetapi ia memerlukan penyelesaian terhadap masalah penyongsangan berskala besar menggunakan kaedah regularisasi yang masih tidak difahami sepenuhnya dan memerlukan penyelidikan lanjut. Kajian ini menyiasat berkenaan pengoptimuman penyongsangan 3D menggunakan data seismik, EM sumber terkawal (CSEM), magnetotellurik (MT) dan data sumur dari pesisir lautan barat laut Borneo. Kesan pemberat regularisasi dikaji dengan melakukan beberapa penyongsangan data MT sintetik yang realistik. Menggunakan pemberat regularisasi yang terbaik, pemberat kecerunan silang yang optimum dijumpai dengan membandingkan hasil penyongsangan MT 3D dengan log resistiviti untuk beberapa nilai pemberat cubaan. Interpolasi log keberintangan menggunakan halaju seismik sebagai pembimbing kedua dipilih sebagai kaedah yang terbaik dalam membina model keberintangan awal. Penyongsangan MT yang dibimbing oleh seismik didapati menghasilkan model yang lebih munasabah berbanding model dari kaedah konvensional. Akhirnya, penyongsangan anisotropik bersama 3D CSEM-MT dan penyongsangan seismik dijalankan. Attribut baru yang diberi nama projeksi seismik-EM (SEMP) telah didefinisikan untuk memberi nilai kualiti bagi takungan yang berpotensi berdasarkan sifat-sifat elastik dan nilai keberintangan. Untuk mengelakkan risiko menjumpai takungan air garam berkeliangan

rendah, kaedah impedans elastik dilanjutkan (EEI) telah digunakan untuk meramalkan keliangan dalam 3D. Attribut SEMP dan EEI telah mengesan beberapa geobodi yang berpotensi sebagai takungan hidrokarbon. Kajian korroboratif geologi seperti geologi struktur dan permodelan sistem petroleum cekungan adalah disarankan untuk lebih memahami geobodi-geobodi ini.

QUANTITATIVE 3D INTEGRATION OF ELECTROMAGNETIC AND SEISMIC DATA TO OPTIMIZE STRUCTURAL SIMILARITY INVERSION RESULTS IN OFFSHORE NORTHWEST BORNEO, MALAYSIA

ABSTRACT

Three-dimensional (3D) inverse modelling of seismic and electromagnetic (EM) geophysical data coupled by the cross-gradient criterion is well known to maximize accuracy and reduce uncertainty in subsurface exploration but this requires solving a large-size inverse problem by regularization methods whose optimization is not fully understood and require further research. This study investigated the optimization of 3D regularized inversion using seismic, controlled source EM (CSEM), magnetotelluric (MT) and well data from offshore northwest Borneo. The effect of regularization was studied by performing several inversions of realistic synthetic 3D MT data. Using the best regularization weight found, the optimal cross-gradient weight was found by comparing 3D MT inversion results against the available resistivity well logs for several trial weights. Interpolation of resistivity logs with seismic velocity as secondary guide was found to be the best approach for building the initial resistivity model. The optimized seismic-guided MT inversion was found to produce a more geologically plausible model as compared to the model from the conventional approach. Finally, 3D anisotropic joint CSEM-MT inversion and seismic inversion were conducted. A new attribute termed the seismic-EM projection (SEMP) was defined to further qualify potential reservoirs based on elastic properties and resistivity values. To avoid the risk of encountering tight brine reservoir, the extended elastic impedance (EEI) approach was used to predict total porosity in 3D. The SEMP and EEI attributes have highlighted several geobodies with hydrocarbon potential. Corroborative geological studies such as

structural geology and petroleum system modelling is recommended to further understand these geobodies.

CHAPTER 1

INTRODUCTION

1.1 Overview

Seismic and electromagnetic (EM) methods are two wavefield methods that are useful in imaging the structure and characterizing the physical properties of the subsurface. Seismic are sensitive to variation in elastic properties, while EM are sensitive to variation in electrical properties, such as resistivity. The elastic and electrical properties can be used to infer bulk properties such as porosity, lithology proportion such as volume of shale and water saturation.

Both seismic and EM data can be acquired on land and marine environments for various applications, such as oil and gas exploration, mineral exploration, and finding groundwater reservoir. Seismic and EM methods have advantages and disadvantages of their own. For exploration in the order of several kilometers beneath earth's surface, seismic method is useful in detecting interfaces between rock beds with different elastic property contrasts at higher resolution than EM method.

However, seismic method is less sensitive to hydrocarbon saturation as compared to EM method. Therefore, there are benefits in interpreting or inverting both seismic and EM methods jointly. The advantages broadly fall into two categories, namely the improvement of subsurface imaging and enhanced characterization of subsurface physical properties (MacGregor, 2020). It is the main thrust of this thesis to investigate and exploit these advantages through integrated interpretation of both seismic and EM methods on a field dataset using novel methodologies.

1.2 Problem statement

EM has relatively poor structural resolution as compared to seismic method. The EM signal bandwidth is smaller than seismic method, and it tends towards low frequency. Hence, its capability to image thin layers is inferior to seismic method. In marine settings, EM surveying is also affected by spatial aliasing since in marine settings, EM receivers are deployed at sparse receiving distance due to cost limitation and limited number of available receivers per survey vessel. Seismic image-guided EM inversion (Zhou et al. 2014; Scholl et al., 2017; Kim et al., 2019; Mackie et al., 2020) is an emerging methodology that has been shown to be effective in producing resistivity models that are structurally consistent with seismic data. However, there are detailed aspects of this approach that are less studied. For example, selection of the values of regularization and structure-constraint weights are often not explained or studied thoroughly.

EM inverse problem is highly nonlinear. Suboptimal inversion parameters & inaccurate forward modelling solution will give inaccurate inversion results. Meju et al. (2018a) shows that depending on the choice of inversion algorithm and regularization methods, the inversion results of a common dataset may vary significantly due to strong non-linearity in EM inverse problem (Figure 1.1). The recovered resistivity structure may not closely follow geological structure and appear to be too smooth. Inadequate or too strong regularization may also cause inversion artifacts that cut across stratigraphic boundaries. Using optimum inversion parameter and including anisotropy in the forward modelling solution (Newman et al., 2010) is expected to improve accuracy and reduce non-uniqueness of the EM inversion results.

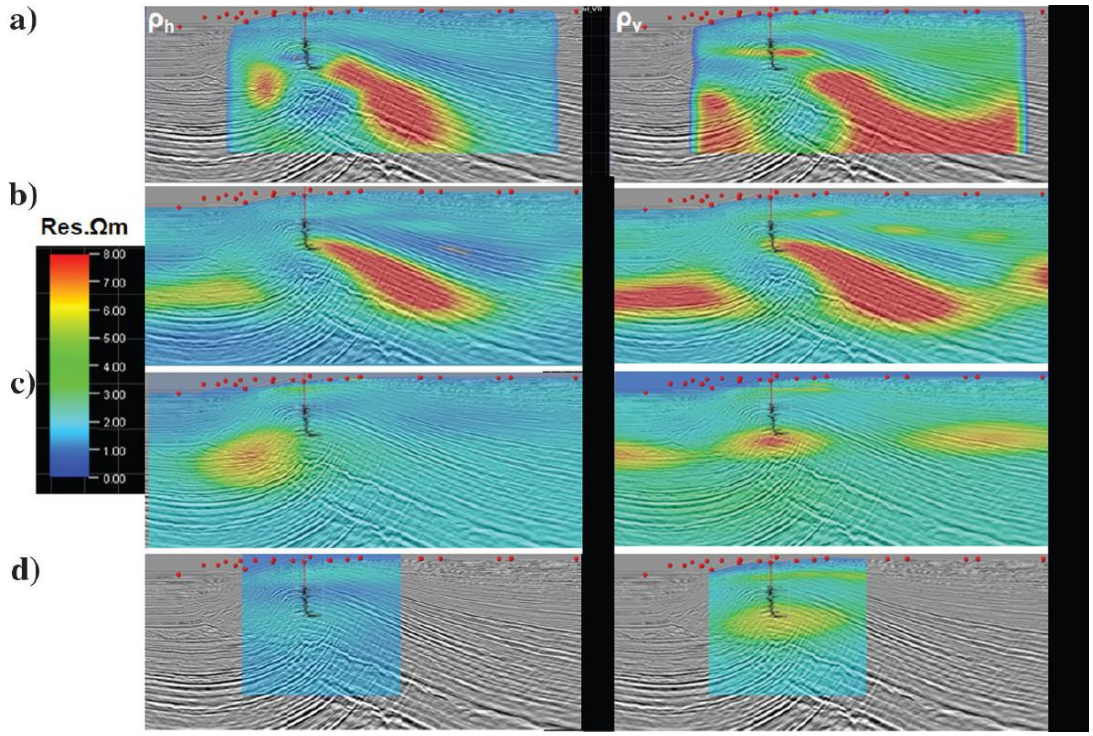

Figure 1.1 Sample results of a blind test of state-of-the-art unconstrained anisotropic (VTI) 3D CSEM inversion technologies available in the oil and gas industry as of January 2017 (Meju et al., 2018a). In each row is shown the ρh and ρv depth sections from different service companies (C1, C2, C3, and C4) for a dip-line passing through the location of an exploration well completed in January 2017, which sampled gas and oil in the bottom part. The coincidentally located seismic image is shown in the background for structural comparison. The standard induction resistivity log is shown at the well location; (a) C1, (b) C2, (c) C3, and (d) C4 models.

It is well known and can be demonstrated by using Gassman fluid substitution (Smith et al., 2003) that seismic amplitude is strongly affected by residual hydrocarbon (Constable, 2010). Low saturation of gas in the pore space will significantly drop the compressional wave (P) velocity (Figure 1.2) and density of rocks hence lowering the acoustic impedance of the rock significantly. Without well data as a reference, brine-bearing sand formation with high porosity, encased by acoustically hard shale can easily be mistaken as class III amplitude versus offset (AVO) response which is represented by seismic amplitude that gets more negative with increasing offset (Rutherford and Williams, 1989). It is sometimes associated with hydrocarbon-bearing sand. Hence, it

represents the key risk in hydrocarbon exploration using seismic data alone. In Figure 1.3, an example is shown where despite two wells having similar amplitude response, one of them encountered gas reservoir, while another one encountered reservoir with residual gas saturation, or fizz gas (O'Brien, 2004). On the other hand, it can be demonstrated based on Archie's equation (Archie, 1942), that resistivity value of porous rock will only increase with high amount of gas saturation (Figure 1.2). Therefore, seismic and EM methods should be jointly interpreted to reduce risk in hydrocarbon exploration (e.g., Hoversten et al., 2021).

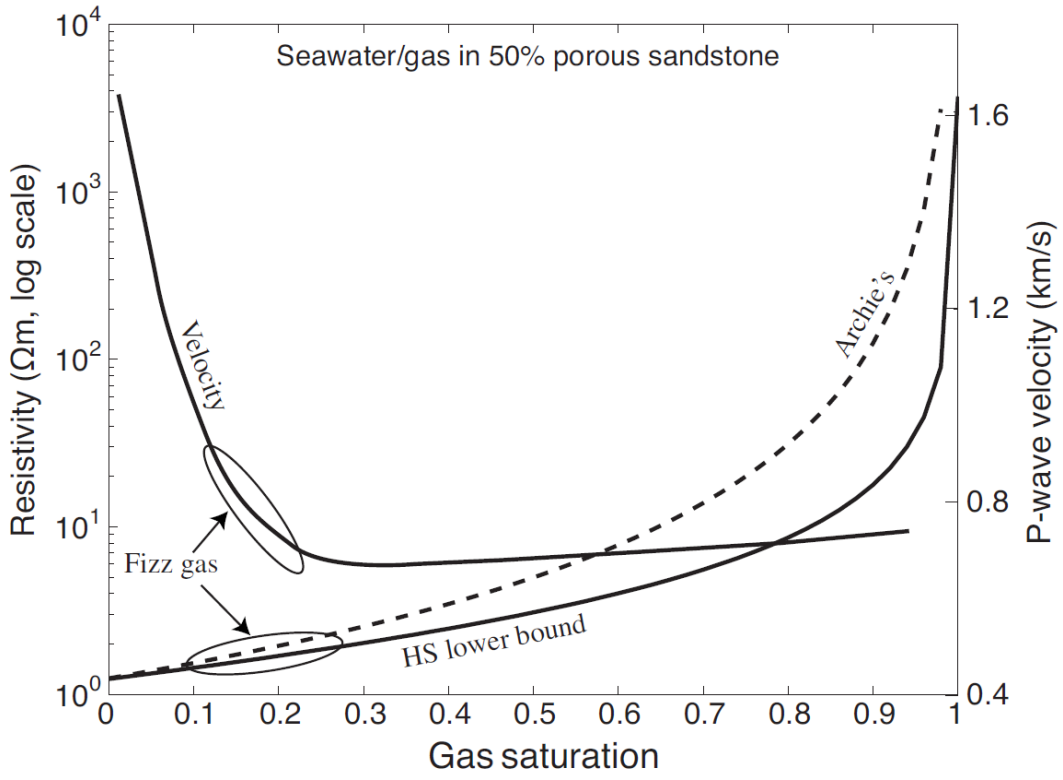

Figure 1.2 Seismic P-wave velocity (from Lee, 2004) and electrical resistivity of a porous (50%) sandstone as a function of gas saturation in the pore fluid (Constable, 2010). The largest effect on acoustic velocity occurs for the first few percent of gas fraction, but disconnected bubbles have little effect on resistivity, which does not increase significantly until gas saturations of 70% to 80% are achieved. The Hashin-Shtrikman (HS) bound is probably the most reasonable mixing law for the resistivity of gas bubbles in water, but Archie's law is provided for reference.

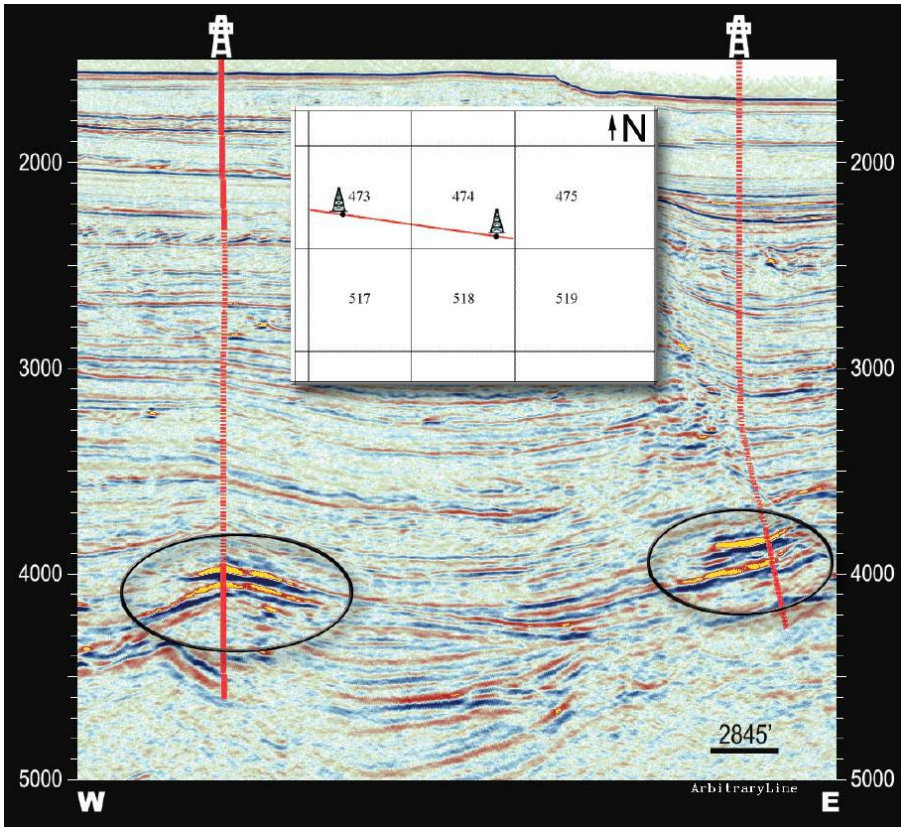

Figure 1.3 Seismic sections showing no significant differences between a discovery well (west) and a well with low gas saturation (east) (O'Brien, 2004).

1.3 Objectives

To address the research problems as elaborated in the previous section, the research objectives are determined as the following:

1.3.1 To optimize the seismic-guided EM inversion workflow

There are several key aspects of seismic-guided EM inversion that requires further optimization. Given that there are several aspects that needs to be optimized, it will be advantageous to perform the test in a systematic, hierarchical manner so that the results are easier to follow. The learnings from this exercise will be useful for any follow up CSEM or joint CSEM-MT inversion.

1.3.2 To improve the accuracy of EM inversion results

In EM forward modelling, more accurate physics should be incorporated, such as by honoring electrical anisotropy. For structural consistency, the ρ_h and ρ_v will be encouraged to be structurally consistent by using cross-gradient constraint (Gallardo and Meju 2003; 2004).

1.3.3 To develop an effective workflow to identify prospective targets using combined application of seismic and EM methods

A semi quantitative approach will be used in the interpretation of the EM and seismic data. Both data types will be inverted separately and then jointly interpreted to locate the zone of interest for exploration drilling.

1.4 Geology of the study area and legacy geophysical datasets

The geology of the study area and legacy geophysical datasets that are available are discussed in this section.

1.4.1 Geology of the study area

The study area is in the fold-thrust belt of offshore northwest Borneo in the South China Sea. The regional setting and the location of the study are shown in Figure 1.4. The water depth in the study area ranges from about 500 to 1600 m. This area is known to has a working petroleum system, as it hosts several commercial hydrocarbon discoveries, such as Gumusut Kakap and Kikeh fields (Abdullah et al, 2018). The sedimentary rocks here are mostly stacks of thin bedded sand in shale characterized by low resistivity and low contrasts (Meju et al., 2019). This region is known to has undergone a complex tectonic history. The structural style here is characterized by

northeast-southwest trending ridges that are formed by elongated thrust anticlines, with intervening mini basins and toe thrust zones (Figure 1.5). The hanging wall anticline with four-way dip closure is the main sought-after trap style for hydrocarbon exploration in this area, while stratigraphic plays remain under-explored. The stratigraphic column for this study area (Jong et al., 2015) is shown in Figure 1.4c. The reservoir targets in this deepwater area are turbidites that are deposited in basin floor system. Six of the turbidite formations are shown in Figure 1.5 as the seismic markers.

1.4.2 Legacy geophysical datasets and well data

This area has been chosen as our study area since it has excellent coverage of EM and seismic data (Figure 1.4b). There are also four wells located in the study area. The EM data were acquired and processed by Electromagnetic Geoservices ASA (EMGS) in 2015 and 2016. Figure 1.4b shows the survey layout of the CSEM-MT survey, seismic survey and well data that are available in this study area. The data acquisition parameters of the CSEM-MT surveys are provided in Appendix D. The combined number of CSEM-MT receivers from both surveys was 647. The 2016 CSEM-MT survey is the densest EM survey ever-acquired in offshore Malaysia.

The seismic data acquisition parameters are given in Appendix D. These parameters were decided based on a pre-survey modelling design to optimize imaging of exploration targets within the survey area. The seismic data uses dual-sensor broadband seismic technology (Widmaeir et al., 2015). The data were acquired and were processed up to Anisotropic Prestack Depth Migration (APSDM) stage by Petroleum Geoservices ASA (PGS ASA). The seismic dataset consists of seismic velocity, fullstack and angle stack data. Other data that were available include seismic horizons and well data from four wells (wells A, B, C, and D). All these data were provided courtesy of PETRONAS for this study.

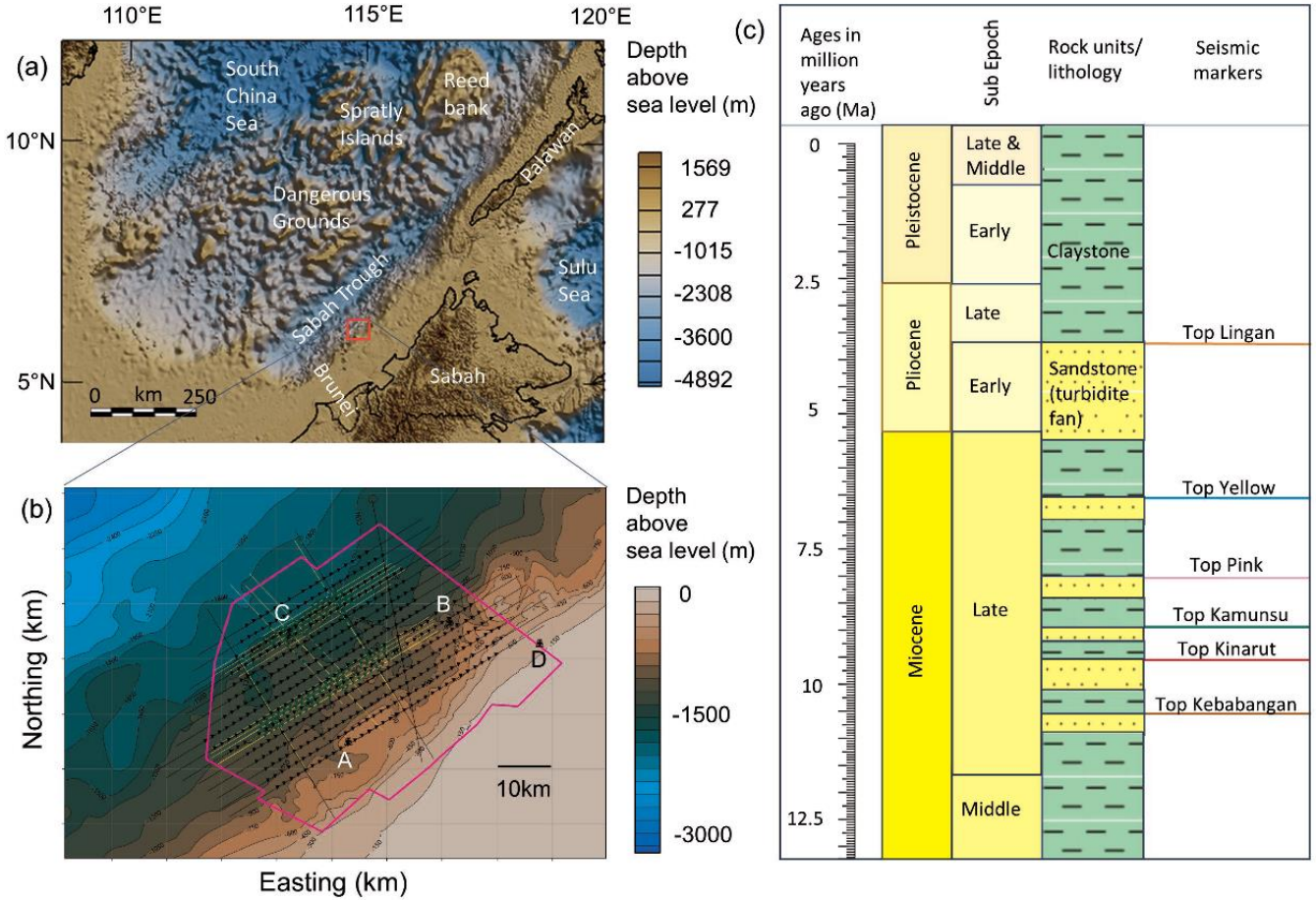

Figure 1.4 (a) Regional setting and study location. Shown are the main physiographic elements in offshore Borneo in southeast Asia. The general bathymetric chart of the oceans (GEBCO - British Oceanographic Data Centre, 2003) is shown in colour. The red box shows the location of our study area, (b) Geophysical survey map of the study area in northwest Borneo, and (c) Stratigraphic column of the study area (after Jong et al., 2015).

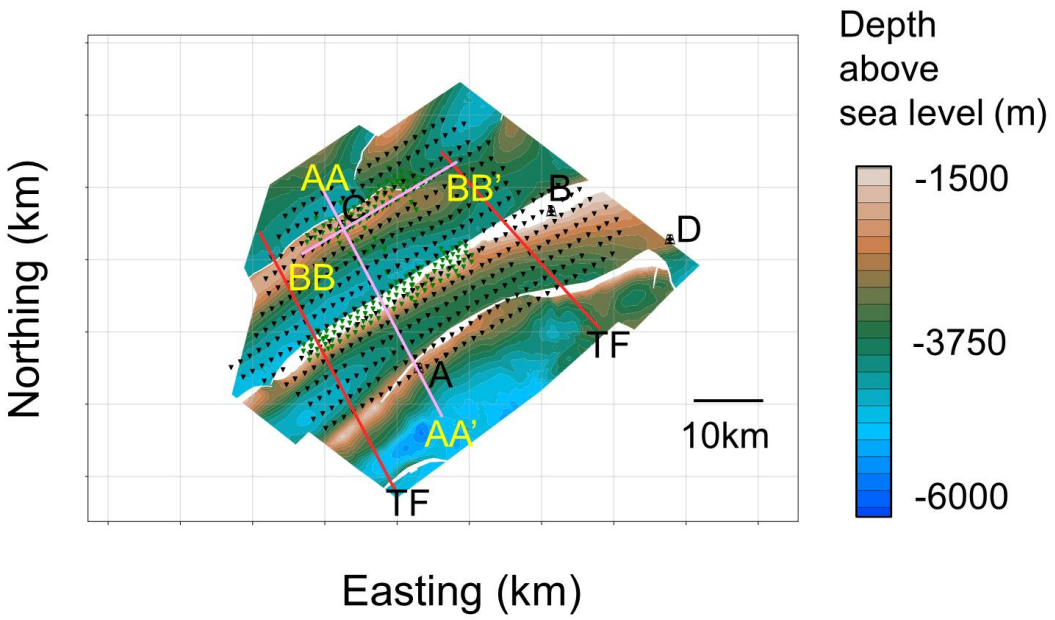

Figure 1.5 Top Kamunsu structural map from seismic data. The grid in the survey map shows the bathymetry (in meters). The inverted triangles in green and black are 2015 and 2016 EM receivers respectively, while the well symbols show the locations of wells A, B, C and D. TF denotes inferred transfer fault separating thrust segments of different relative motion. AA to AA' and BB and BB' are the dip line and strike lines respectively, where the inversion results shall be shown later.

1.5 Scope of study

The scope of this study includes the integrated interpretation of 3D EM (CSEM and MT), seismic, and well log data. Emphasis is given on the study of geophysical inversion and optimization of the key components of the inversion, such as regularization and cross-gradient weights, initial model, and input data. Among the inversion approach being studied are seismic-guided 3D MT inversion, joint 3D CSEM-MT inversion, and seismic inversion. The scope includes development of novel, integrated seismic and EM data interpretation approach. Finally, the scope includes the interpretation of the inversion results in terms of regional and local geology for

hydrocarbon prospecting in an area with complex, fold-thrust structures in deepwater offshore Northwest Borneo.

1.6 Novelty and significance

The hierarchical workflow of selecting optimal seismic guided EM inversion workflow is novel. Among the crucial part of the workflow are the selection of the regularization weights based on field-realistic synthetic model. It is a more objective method for determining the weights, as compared to other conventional approach such as analysis of L-curve (Hansen, 1992) that has been shown to be subjective (Constable et al., 2015). The cross-gradient weight was also found to ha have significant impact on the inversion results. Using well resistivity logs as calibration, optimal cross-gradient weight was derived for this study.

Another novel aspect of this study was the use of seismic velocity as secondary guide to interpolate resistivity log during initial resistivity model building. This approach was shown to produce superior result as compared to the other options, based on the comparison of the results with well logs, convergence, data misfit analysis. This approach is reasonably simple and does not require complex rock physics relationship. Another advantage of this approach is that it produces a 3D resistivity model that is structurally consistent with the seismic velocity, which will be beneficial for any joint seismic and EM interpretation process.

A new seismic-electromagnetic projection (SEMP) attribute was proposed through a combination of SI-AI projection and log (resistivity). The SEMP attribute is novel, and further improves the pay sand facies separation from non-pay facies based on well log data. Extended elastic impedance (EEI) attribute (Whitcombe, 2002) was

also applied to produce total porosity volume as a secondary attribute to further polarize the delineated targets. The interpretation results correlate well with the observations from the three wells available in the study area. Several prospective targets, residing at structural flanks and synclines were identified by using the SEMP attribute in 3D geobody analysis.

1.7 Thesis outline

This thesis started in Chapter 2 by reviewing the fundamental aspects of MT, CSEM and seismic methods. Previous studies related to the integration of EM and seismic methods, forward and inverse theory, acquisition and processing of MT, CSEM and seismic data were reviewed. In Chapter 3, a summary was given on the location and geology of the study area, data availability and the software and hardware used for this study. Then, the methodology for optimization of seismic-guided 3D MT inversion, joint CSEM-MT inversion, seismic inversion and the integrated interpretation approach were explained. In Chapter 4, the results were presented, analyzed and discussed following the order as described in methodology. Finally, this thesis concludes in Chapter 5 where overall summary and recommendation for further improvement in future studies are given.

CHAPTER 2

LITERATURE REVIEW

2.1 Introduction

In this chapter, literature on geology and petroleum system of the study area will be reviewed first, followed by some preliminaries on MT, CSEM and seismic methods shall be reviewed. The related forward and inverse theories that are necessary to estimate electrical and elastic models given the input data shall also be reviewed. Finally, the CSEM, MT and seismic data acquisition and processing aspects shall be discussed.

2.2 Petroleum geology of the study area

Some of the key elements of the petroleum system in this study area are discussed in this section.

2.2.1 Stratigraphy and structural geology

The source of sediment input to the study area is suggested to start during early Miocene, when Crocker fold-thrust was uplifted and exhumed due to series of deformation events (Kessler and Jong, 2015). During this time, West Crocker formation was exposed onshore and eroded. The resulting sediments were then transported offshore as prograding clastic deltas (Jong et al. 2016). The deepwater offshore Sabah basin are a complex interplay of turbidite sands and hemipelagic shales, interbedded with Mass Transport Deposits (MTDs) resulting from episodes of major slope failure (Jong et al., 2016).

NW Sabah is dominated by numerous structural trends of tightly folded and thrusted Miocene to Pleistocene sediments forming the Sabah deepwater fold-thrust belt, resulting from the complex interaction between gravitational forces and compressional tectonics (Legrand et al. 2015; Khamis et al., 2018). The turbidite sand deposition that occurs in deepwater can be divided into pre-kinematic, syn-kinematic and post kinematic phases by understanding the structural evolution of the study area. Turbidite sands that are deposited during pre-kinematic period tend to be unconfined. Meanwhile, turbidite sands that are deposited syn- and post-kinematic are usually confined between structural ridges, forming ponded turbidites (Khamis et al., 2018). This understanding of turbidite fans depositional pattern variation based on geological age is important in facies modelling in the study area.

Through structural restoration study (Figure 2.1), it was determined that the deformation history of the study area could be separated into two main kinematic phases, which are pre-kinematic and syn-kinematic (Jong et al., 2015). Pre-kinematic phase occurs during approximately middle Miocene (equivalent to Kinarut and Kebabangan fan deposit), during which high sediment influx caused slope failures that creates mass transport complex (MTC) that were mobilized to deepwater (Jong et al., 2015). Then, the MTC was underlain by the Kinarut fan. Then, in syn-kinematic phase from mid-late Miocene to early Pliocene (equivalent to later time of Kamunsu fan deposition) the toe-thrust anticlines were formed in the deepwater environment with turbidites deposition in confined settings and ponded turbidites (Jong et al., 2015). The pre- and post-kinematic period are separated by the Shallow-Regional Unconformity (SRU) that is aged about 8.5 Ma.

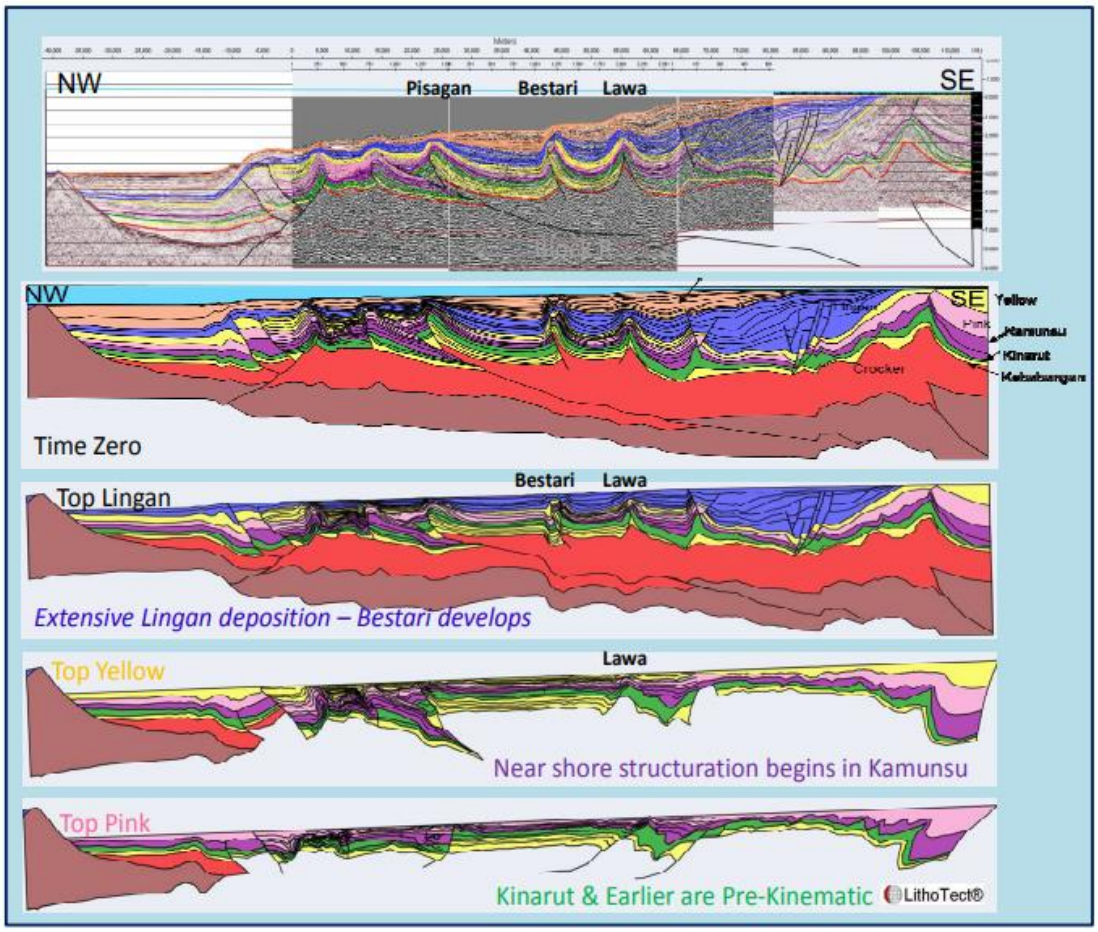

Figure 2.1 Deformation history of Sabah fold-thrust belt (Jong et al., 2015). Note that structuration in the outboard area continued to recent times, while in the inboard/proximal area deformation has ceased around top Lingan times.

2.2.2 Petroleum system

In our study area, the reservoir targets are the turbidite fans. MTD shales below Kebabangan fan is the primary source rock, aside from shales below Kamunsu and Kinarut turbidite fans (Jong et al., 2015). Understanding the timing of sedimentation, trap formation and hydrocarbon generation and expulsion is critical in assessing risk and probability of success of a prospect. From basin modelling study (Jong et al., 2014), it was determined that the expulsion of the hydrocarbon occurs after the trap has been formed (Figure 2.2). Hence, it was decided that the petroleum system in this study area is working, as evidenced by several successful drilling around this study area.

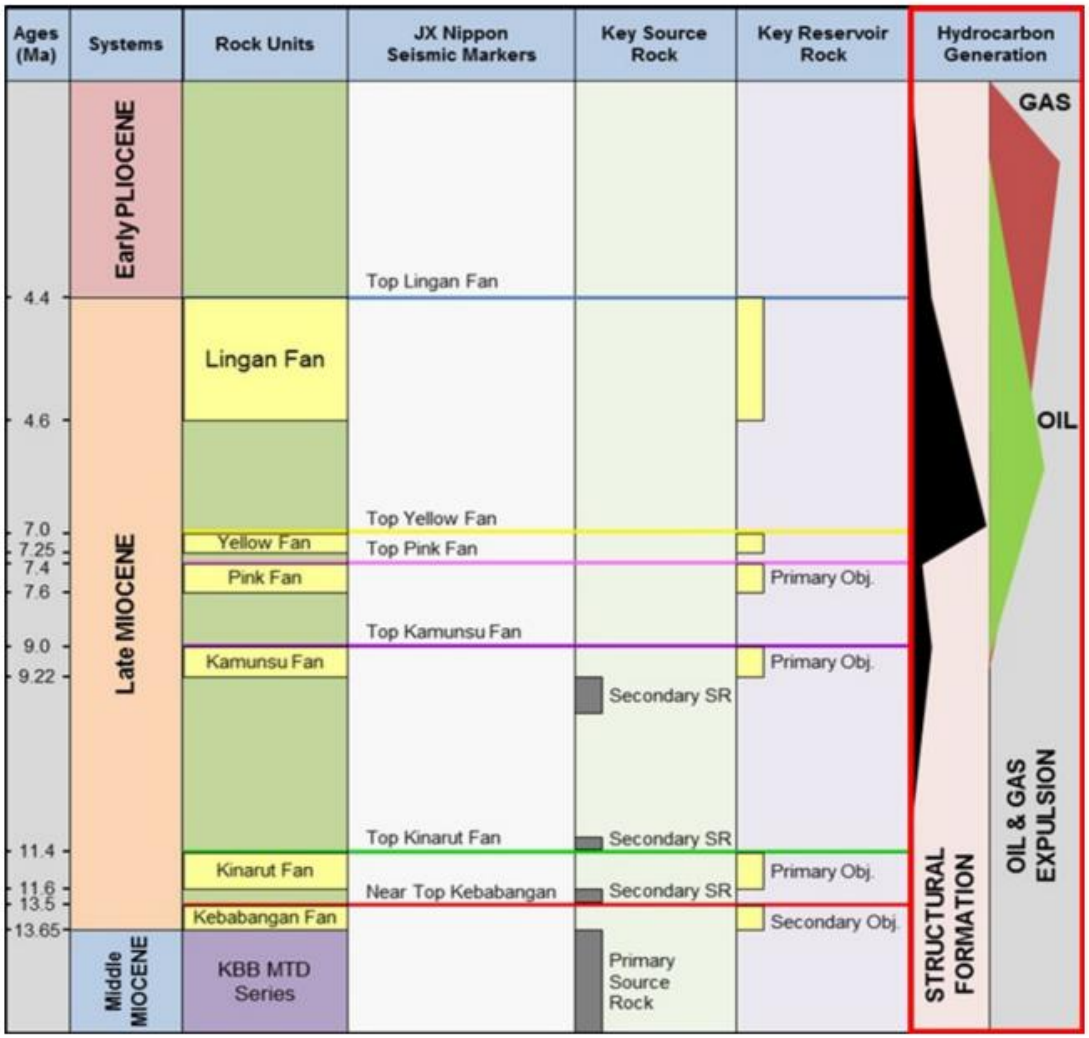

Figure 2.2 Peak oil and gas generation in the study area took place after the toethrust structures were well-developed, thereby providing a favorable timing for HC trapping and oil/gas accumulations (Jong et al., 2015).

2.3 Preliminaries on MT, CSEM and seismic methods

Since MT and CSEM are both of EM methods, the physics of both methods are governed by the Maxwell's equation (equations 2.1 to 2.4). Meanwhile, the physics of seismic method is governed by the elastic wave equation (Robinson and Clark, 2017). Brief overview of MT, CSEM and seismic method are discussed in the following sections.

2.3.1 MT method

MT method is a passive, inductive EM method that uses naturally occurring magnetic fields as its source (Cagniard, 1953; Chave and Jones, 2012). At short period, the signal comes from lightning discharges (also known as sferics) at equatorial region which travels in between ionosphere and earth's surface as wave guide. At short period, the signal comes from interaction between solar wind and earth's magnetosphere. There is a frequency band with reduction in MT signal which is termed as dead band between 0.1 to 10 Hz. The MT source spectrum is shown in Figure 2.3 The time varying magnetic field induce currents in the subsurface, which is more conductive as compared to the very resistive air. The interaction of the telluric current with the subsurface produce measurable electric and magnetic fields at the earth surface that contain information about the subsurface conductivity, or its inverse, resistivity structure. MT is an inductive EM method and hence is preferentially more sensitive to conductors.

The MT data are routinely acquired on land and marine for various purposes. For example, it is useful for tectonics (e.g., Maurya et al., 2018; Bai et al., 2010), geothermal (e.g., Maryanto et al., 2017; Soyer et al., 2018), carbon capture and sequestration (Streich, et al., 2010), and hydrocarbon exploration (e.g., Meju et al., 2018a, 2018b). On land, the setup of MT survey consists of two orthogonal electric dipoles that are oriented North-South and East-West respectively (Figure 2.4). Three magnetic induction coils that records x, y and z components of the magnetic fields are used and buried to avoid noise. The electric dipoles and the coils are connected to data logger. Remote reference receiver that measures horizontal magnetic field is used to perform remote reference processing to remove correlated noise (Gamble et al., 1979). On marine case, the MT data is often acquired with CSEM data, although it can be acquired independently.

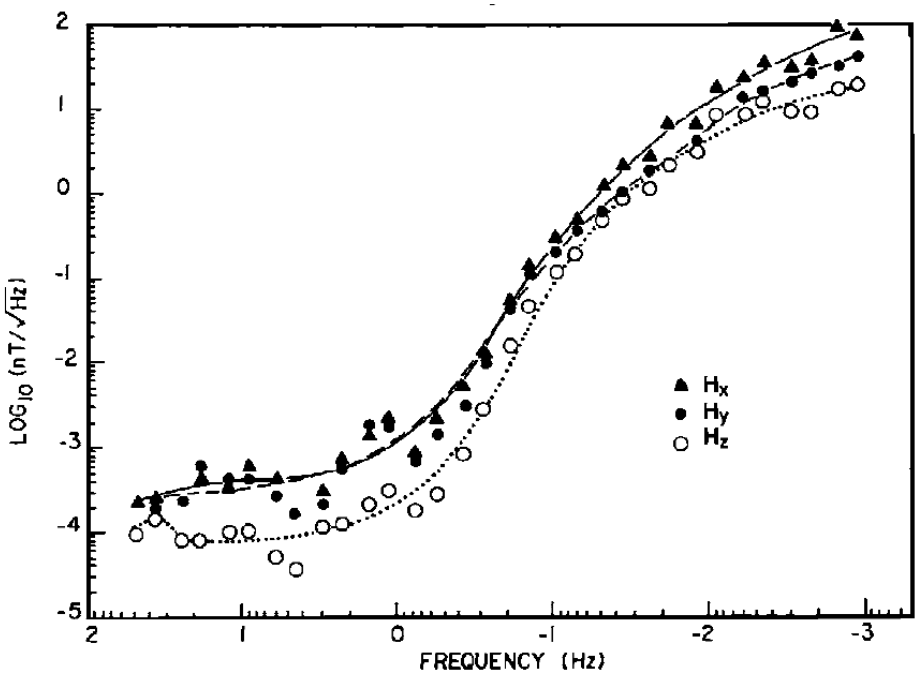

Figure 2.3 Typically observed magnetic field amplitude spectrum (Vozoff, 1991).

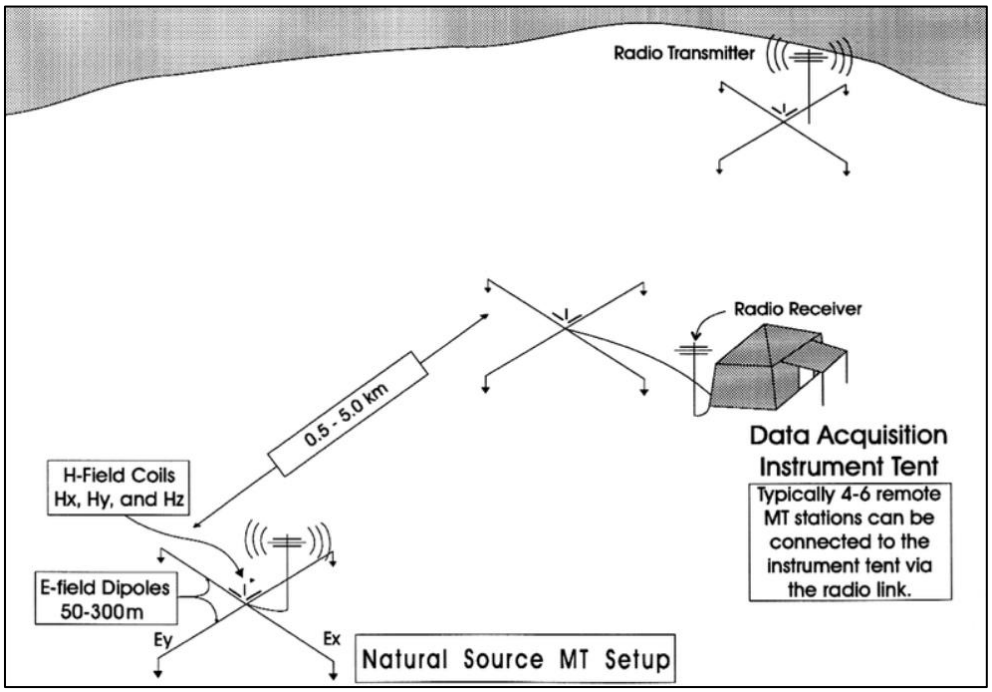

Figure 2.4 Setup of magnetotelluric survey on land (Ostrander, 1999). Two electric dipoles are laid orthogonal to each other and oriented North-South and East-West, connected to the instrument tent via radio link and sometimes trenched in to minimize noise. Three components induction coils are connected to the data logger and buried in the ground to minimize noise arising from wind and ground vibrations due to vehicular traffic.

2.3.2 CSEM method

The CSEM method uses artificial sources. Controlled Source Audio Magnetotellurics (CSAMT) (Goldstein and Strangway, 1975) and transient or time domain EM (TEM) (Nabighian, 1979) are examples of CSEM methods that are applied on land. For CSAMT, remote grounded dipole is used as EM signal source. The resulting CSAMT data are interpreted in similar way to the passive MT method. For TEM, time-varying current is supplied into ungrounded transmitter loop. Then, it is rapidly turned off to generate rapidly changing magnetic fields that will induce eddy current in the ground. The eddy currents will flow in conductive bodies and generate secondary magnetic field that decays with time. The rate of decay of these magnetic fields are recorded as voltages induced in the receiver loop. Good conductors produce magnetic field that decay rapidly and vice versa.

In marine environments, there are several variants of CSEM surveying systems that are available (Figure 2.5) (MacGregor and Tomlinson, 2014). The standard configuration in Figure 2.5(a) uses a horizontal electric dipole (HED) source towed above the seafloor, while the EM receivers are deployed at the seafloor. Configuration in Figure 2.5(b) is a variant of Figure 2.5(a) where three-component EM receivers are put behind the HED source up to 1 km offset. The configuration in Figure 2.5(c) uses a linked HED source and EM receivers towed at depth of about 10 to 100 meters from sea surface, with source-receiver offset from 500 to 8000 meters (Mattsson et al., 2012). Finally, configuration Figure 2.5(d) uses sources and receivers that are vertical electric dipole (VED). Out of these configurations, Figure 2.5(c) is the most operationally efficient and has the closest inline receiver spacing. It is also possible to simultaneously acquire two dimensional (2D) seismic while acquiring EM data in this configuration (Engermark et al., 2014). However, configuration Figure 2.5(c) inherently lacks in

azimuthal coverage that is needed to resolve horizontal resistivity. It is also suitable only for shallow water environment of about 20 to 400 meters water depth. Constable et al. (2012) describes configuration Figure 2.5(b) as suitable for primarily mapping shallow seafloor, since it uses only 1 km source-receiver offset. The shallow seafloor features of interest include gas hydrates and shallow gas, which are considered as drilling hazards. When rugose seabed is present, it will be challenging to implement the Figure 2.5(b) configuration. Configuration Figure 2.5(d) systems using VED sources and receivers (Holten et al., 2009) is the most difficult to implement operationally. Only small tilt angles can be tolerated for the source and receiver, to avoid the horizontal electric field from dominating the response as the vertical electric field is small. The receivers are either using extensible tripod or buoy with strong buoyancy, while the source electric dipole is attached to the vessel and positioned accordingly to ensure that the verticality condition is met. Movement of the whole sources and receivers is operationally difficult, especially because the extensible tripod is huge in size. Although the usable offset from Figure 2.5(d) configuration is relatively short (about 500 to 1500 meters), it has been shown from modelling (Cuevas and Alumbaugh, 2011) that the VED system is able to resolve resistive subsurface layers at shorter offset as compared to the HED system. Hence Figure 2.5(d) configuration has potential to improve the subseafloor resistivity lateral resolution (MacGregor and Tomlinson, 2014). The marine CSEM acquisition setup shown in Figure 2.5(a) is widely used, where a HED dipole source is towed at about 30 meters from seafloor and EM receivers are deployed at the seafloor. This configuration has the advantage to be easily setup for 3D survey, which provides data with good azimuthal coverage, which then increases the data sensitivity to horizontal resistivity. This configuration is used for acquisition of CSEM and MT data for this study and will be discussed in more detail in section 2.5.1.

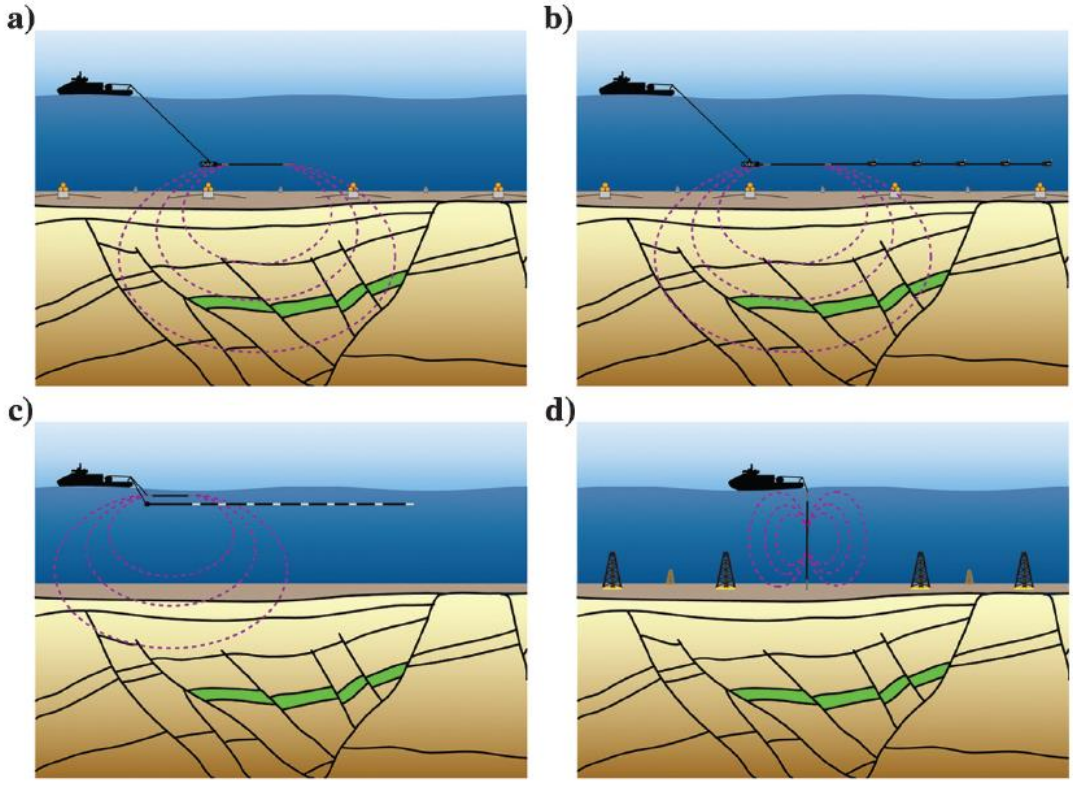

Figure 2.5 Schematic diagrams showing various CSEM acquisition systems (Macgregor and Tomlinson, 2014). (a) Standard CSEM acquisition with a horizontal towed source and seafloor deployed receivers. (b) A variation on the standard in which a 1 km streamer of three-component receivers is deep-towed behind the source. (c) Streamer CSEM acquisition in which the source and receiver are towed behind the survey vessel. (d) Vertical electric dipole acquisition.

2.3.3 Seismic reflection method

Seismic reflection method is the most routinely used geophysical method in hydrocarbon exploration. Seismic sources such as airgun in marine, and explosive or vibroseis on land, are used to produce seismic waves that are reflected and transmitted at geological formation boundaries (Figure 2.6). On land, the receivers are typically geophones which records compressional (P) waves. Shear (S) wave recording is also possible using three-components geophones.

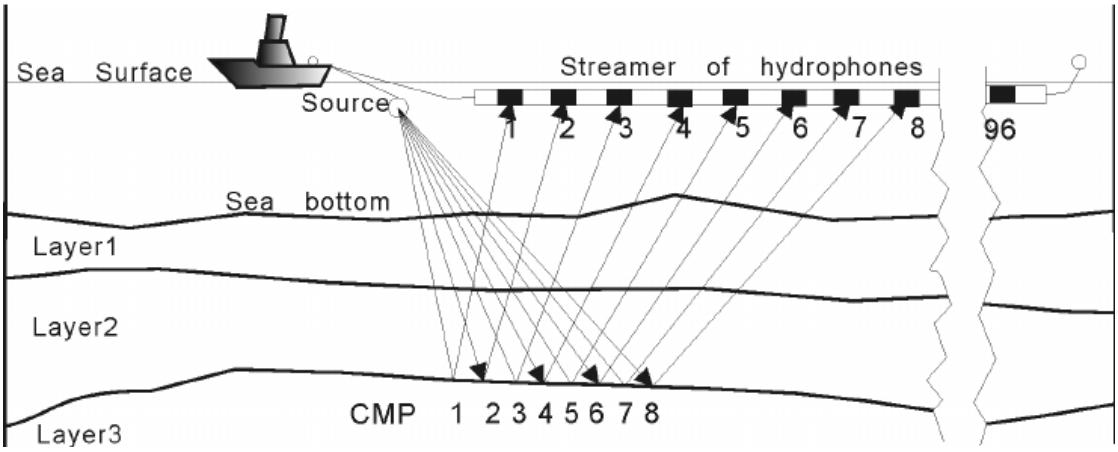

Figure 2.6 Marine seismic survey configuration. The source signals from the airgun penetrate the subsurface and are reflected at geological formation boundaries, travel up to surface and is finally recorded by the hydrophones encased in the streamer (Song et al., 2012).

In marine environments, streamers containing regularly spaced hydrophones are used to record P-wave (Figure 2.6). In special case, a receiver unit can have both hydrophones and geophones as in the case of dual sensor streamer (Widmaier et al., 2015), and ocean-bottom cable (OBC) or ocean-bottom node (OBN) systems (e.g., Akalin et al., 2014; Farfour and Yoon, 2016). The dual sensor streamer technology (also known as GeoStreamer^{TM}), a proprietary technology by PGS was utilized in this study and will be discussed in more detail later.

2.4 Previous studies

In this section, previous works related to the research objectives of this study are reviewed.

2.4.1 Image-guided EM inversion

In image guided EM inversion (Zhou et al., 2014; Scholl et al., 2017; Kim et al., 2019; Mackie et al., 2020), structural information is derived from collocated auxiliary

data and used as a soft constraint in the EM inversion process. The structural information is provided in the form of structure tensor (Knutsson, 1989) derived from two-dimensional (2D) cross section or three-dimensional (3D) cube which contains structural geology information of interest. It improves structural consistency of the resulting inverted resistivity models to the presumed subsurface structure. It also restrict the number of possible models and in effect reducing the uncertainty in the inversion process.

Zhou et al. (2014) performed 2D DC resistivity inversion using guiding-image from ground penetrating radar (GPR) for hydrogeological study. They concluded that the result is more acceptable in hydrogeological sense as compared to the conventional inversion. Scholl et al. (2017) presented two case studies of image-guided inversion from land and marine environments using airborne EM and marine CSEM, respectively. For the land case study, they used outcrop observation to constrain the shallow structures of the inversion result. They concluded that the guided inversion produced resistivity structure that is more geologically realistic than the standard inversion result obtained using smoothness constraint only.

Mackie et al. (2020) applied seismic guided MT and CSEM inversion on the same 3D field dataset used in this study. They found that the seismic-guided inversion result was comparable to the inversion that used seismic horizons as tear surfaces (Figure 2.7). Hence, using this approach increase efficiency and accuracy since horizon picking is not required, and possible human error in picking seismic horizons can be avoided. However, it was noted that the effect of varying key parameters in seismic-guided EM inversion such as regularization and cross-gradient weights and choice of initial model were not investigated in detail.

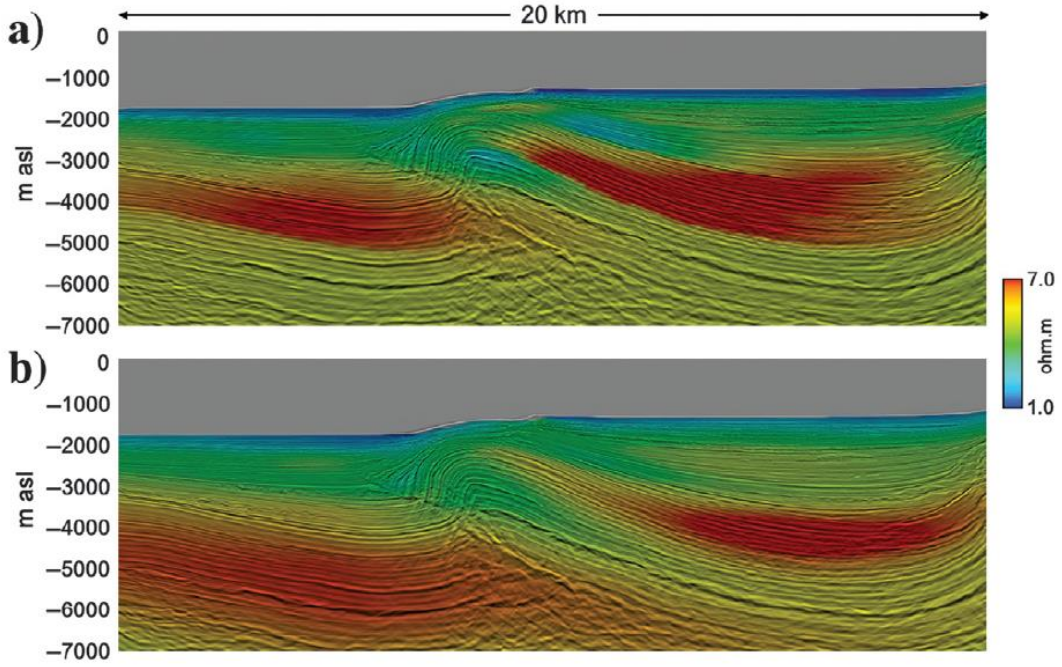

Figure 2.7 Comparison of results of using seismic horizons (tear surfaces) and structure tensors in anisotropic CSEM inversion (Mackie et al., 2020). (a) Conventional constrained inversion using horizons as tear surfaces as hard constraints. (b) Seismic image guided joint CSEM and MT inversion.

Determination of optimal weighting factors for various constraints is an important aspect in image-guided inversion. Peng et al. (2019) applied cooperative seismic and MT inversion of synthetic data using cross-gradient constraint. They performed sub-iteration inversion to choose cross-gradient weight for each iteration and selected the weight that produced the least data misfit. However, it has been shown that having least data misfit does not guarantee unique solution (Meju et al., 2018a). Robertson et al. (2020) studied various aspects in 3D MT inversion such as the regularization weights and choice of the initial model. They found that the regularization weight affects the inversion result significantly. However, their study is regional in nature and did not consider seismic and well log data as a priori information. Hoversten et al. (2021) performed seismic-guided CSEM inversion of CSEM data and determined the cross-gradient weight using well log as control data. They founded that seismic-guided CSEM inversion with optimal cross-gradient weight gives resistivity

that matches the resistivity log. It is noted that testing of cross-gradient weight using CSEM data is compute intensive due to high data density and will need to be made more efficient.

Based on the above studies, more objective criteria are needed in determining the regularization and cross-gradient weights for seismic-guided. Aside from that, a more efficient method is needed in evaluating the inversion parameters. In this study, well logs, section analysis and comparison with seismic structure shall be used in determining the weights. Inversion parameter testing shall also be done using MT data as inverting MT data is much more efficient than inverting CSEM data.

2.4.2 Improvements in EM inversion accuracy

The importance of honoring anisotropy in CSEM modelling has long been recognized (e.g., Tompkins et al., 2004). Advances in numerical modelling allowed anisotropy to be included in forward and inverse modelling successfully (Newman et al., 2010). However, in some inversion results, structural inconsistency between horizontal resistivity (ρ_h) and vertical resistivity (ρ_v) have been observed which are geologically not plausible (Figure 1.1). Meju and Fatah (2017) suggested that cross-gradient constraint between can be applied to encourage the structural similarity between the ρ_h and ρ_v inverted models. Meju et al. (2019) formulate the problem for the non-linear cross-gradient constrained anisotropic CSEM inversion and its solution for small- and large-scale problems. If collocated seismic data is available, linear cross-gradient constraint can be applied by encouraging the inverted ρ_h and ρ_v structures to follow the seismic structure (Mackie et al. 2020) as have been explained in section 2.3.1. However, selection of optimum cross-gradient weight is often done in either subjective or heuristic manner.